

Multigrid Methods for Open Boundary Problems in Geophysics

A. Plaks, I. Tsukerman, S. Painchaud, and L. Tabarovsky

Abstract—The proposed numerical procedure for static open boundary problems combines fast adaptive multigrid methods with spatial mappings of the infinite region to a finite computational domain. A rigorous analysis of the finite element solution error for ballooning and for spatial mappings is presented. The method is applied to geophysical problems of dc logging.

Index Terms—Error analysis, finite element methods, geophysical measurements, iterative methods.

I. INTRODUCTION

LARGE 3-D Finite Element (FE) problems require significant computational effort, and the efficiency of numerical algorithms is of paramount importance. Unbounded problems present additional challenges and require special treatment. Toward this end, we propose a combination of spatial mappings with fast adaptive multigrid solvers. The paper has the following novel features:

- 1) An algorithm combining general domain mapping techniques for open boundary problems with fast adaptive multigrid methods.
- 2) A rigorous accuracy comparison of coordinate transformation methods with competing techniques.
- 3) Applications to geophysical problems of dc logging.

Special emphasis is placed on the second item on the list above. A variety of methods have been proposed for open boundary problems in the FE context; see e.g. the extensive survey [1]. Broad categories of such methods include hybrid FE—boundary element algorithms, infinite elements, spatial transformations, and Perfectly Matched Layers (PML). Typically, research papers present the advantages of their respective methods, but to the best of our knowledge, there has been no rigorous theoretical comparison of the accuracy of different techniques. A careful analysis of all proposed methods would not be possible in one short paper; instead, we highlight the main principles on which a rigorous evaluation of the methods should be based. As typical and important examples, we study the errors of the method of ballooning and of the method of spatial mappings. Infinite elements (e.g. [2]) would also be

interesting to analyze along these lines, but this remains out of the scope of the present paper.

II. PRECONDITIONED ADAPTIVE MULTIGRID SOLVERS

Traditional iterative and direct solvers (such as ICCG, Nested Dissection, Quotient Minimum Degree and others) are not efficient for 3-D meshes with several millions elements or more. For example, ICCG, currently one of the most popular solvers, requires asymptotically $O(n^{4/3})$ arithmetic operations for 3-D problems (n is the number of nodes in a FE mesh).

The best multigrid methods are much more efficient. The computational time and memory for the Bramble–Pasciak–Xu (BPX) preconditioner [3], [4] is typically $O(n \log^\beta n)$, $\beta \geq 0$. In practical terms, this results in a significant reduction of the computational cost. Further improvement is possible by combining the BPX preconditioner with adaptive mesh refinement. Details of the algorithm have already been presented [5] and will not be repeated here.

The algorithm implemented in this paper combines the domain mapping of [6] (Section III) with a BPX-preconditioned adaptive multigrid scheme.

III. SPATIAL MAPPINGS AND PERFECTLY MATCHED LAYERS

A. Coordinate Mappings and Material Characteristics

The infinite exterior region can be mapped onto a finite domain and then handled with regular finite elements. This well-known approach has the advantage of preserving the usual properties of the FE method (such as sparsity of the stiffness matrix and its positive definiteness for static problems). A coordinate transformation sufficiently general for many practical purposes was proposed by Stochniol [6].

Following [6], we introduce two auxiliary artificial boundaries Γ_0 and Γ_∞ (Fig. 1) described by functions $R_0(\theta, \varphi)$ and $R_\infty(\theta, \varphi)$, respectively, in the spherical system.

A suitable spatial transform that maps the infinite exterior region Ω_{ext} outside Γ_0 onto a finite band between Γ_0 and Γ_∞ is sought in the form

$$\tilde{r}(\theta, \varphi) = a(\theta, \varphi) + b(\theta, \varphi)/r(\theta, \varphi)$$

with yet undetermined coefficients a , b . If Γ_0 gets mapped onto itself and infinity gets mapped onto Γ_∞ , then $a = R_\infty$, $b = (R_0 - R_\infty)R_0$, and

$$\tilde{r} = R_\infty - \frac{(R_\infty - R_0)R_0}{r} \quad (1)$$

We consider a dc current (or, almost equivalently, an electrostatic) problem of the form

$$\nabla(\sigma \nabla u) = 0 \quad (2)$$

Manuscript received October 25, 1999. This work was supported in part by the National Science Foundation and by Baker Atlas, Inc.

A. Plaks and I. Tsukerman are with the Electrical Engineering Department, the University of Akron, Akron, OH 44325-3904 USA (e-mail: {aplaks; itsukerman}@uakron.edu).

S. Painchaud and L. Tabarovsky are with Baker Atlas Inc., 10201 Westheimer, Houston, TX 77042 USA (e-mail: {Stephen.Painchaud; Lev.Tabarovsky}@waii.com).

Publisher Item Identifier S 0018-9464(00)05006-8.

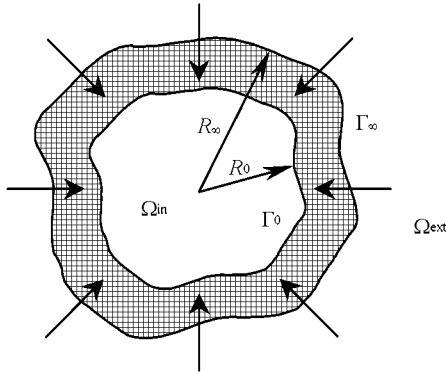


Fig. 1. The spatial mapping.

with appropriate boundary Dirichlet and/or Neumann conditions, where σ can be a tensor. The weak formulation of this problem is

$$\int_{\Omega} \sigma \nabla u \cdot \nabla u' d\Omega = 0,$$

with both the solution u and the “trial” function u' satisfying the relevant Dirichlet conditions.

For the weak formulations of the dc current problem in the original and transformed domains Ω and $\tilde{\Omega}$ to be equivalent, one must have

$$\int_{\Omega} \sigma \nabla u \cdot \nabla u' d\Omega \equiv \int_{\tilde{\Omega}} \tilde{\sigma} \tilde{\nabla} \tilde{u} \cdot \tilde{\nabla} \tilde{u}' d\tilde{\Omega} \quad (3)$$

Denoting with J the Jacobi matrix $(\partial(x_1, x_2, x_3)/\partial(\tilde{x}_1, \tilde{x}_2, \tilde{x}_3))$ of the spatial mapping, treating the gradients in (3) as column vectors in R^3 and the conductivity tensors as 3×3 matrices, one has $\tilde{\nabla} \tilde{u} = J \nabla u$, so the left hand side of (3) becomes

$$\begin{aligned} \int_{\Omega} (\nabla u')^T \sigma \nabla u d\Omega &= \int_{\tilde{\Omega}} (J^{-1} \tilde{\nabla} \tilde{u}')^T \sigma (J^{-1} \tilde{\nabla} \tilde{u}) |J| d\tilde{\Omega} \\ &= \int_{\tilde{\Omega}} (\tilde{\nabla} \tilde{u}')^T J^{-T} \sigma J^{-1} \tilde{\nabla} \tilde{u} |J| d\tilde{\Omega}, \end{aligned}$$

from which it immediately follows that the conductivity tensor must be transformed as [6]

$$\tilde{\sigma} = J^{-T} \sigma J^{-1} |J| \quad (4)$$

B. Coordinate Mappings and Perfectly Matched Layers

Perfectly Matched Layers (PML) are widely used to model wave propagation. Actually, two quite different approaches are disguised under the common name of PML. Berenger’s approach [7] is based on an artificial modification of Maxwell’s equations in a fictitious absorbing layer, and cannot be incorporated into FEM in a natural way (in addition, stability problems have been reported [8]).

More promising in the FE context is the method due to Sacks *et al.* [9]. A layer of a fictitious absorbing material, with complex permittivity and permeability, is introduced. It turns out that for suitable material parameters the reflection coefficient can be made zero for all angles of incidence of a plane incident wave.

Recently PML’s were applied to electro- and magnetostatic problems [10]. However, the analysis and the boundary

conditions used in [10] are based on the implicit assumption that the potential decays exponentially with distance,¹ which is generally not true. The PML for static problems is little more than the equivalent coordinate mapping (e.g. $\tilde{x} = ax$), in the case of [10], equivalent to transforming the permittivity tensor as $\tilde{\epsilon} = A\epsilon$, $A = \text{diag}(a, 1, 1)$ (see Section III-A). This does not result in any exponential decay, however.

IV. ACCURACY ESTIMATES

A. The Key Question: Approximation Accuracy

The key question for a rigorous comparison of different methods, such as ballooning [1], spatial mappings [6], etc., has apparently not been clearly stated so far, at least in the literature on computational electromagnetism. Which approach provides a *more accurate FE approximation* of the exact solution? This question warrants a careful study that appears in part in the subsequent sections.

Since domain mappings may be viewed just as variable changes, they do not automatically improve the accuracy. (There is no reason for one set of coordinate variables to be intrinsically better than the other.) In fact, solutions in the original and transformed domains would be completely equivalent *if finite elements were also transformed* (making these elements infinite in the exterior region).

In practice, however, elements do not get transformed (both the original and the transformed domain are subdivided, for example, in tetrahedra), and it is for this reason that spatial mappings are not equivalent to, say, the methods of “ballooning” [1].

B. An a priori Accuracy Estimate for Ballooning

Consider the following common setup for the method of “ballooning” (Fig. 2). In the exterior region, m spherical shell layers $\Omega_i (1 \leq i \leq m)$ of elements with increasing radii $r_0 < r_1 < \dots < r_m$ are introduced.

To obtain a *qualitative a priori* error estimate, we take several simplification assumptions that make the analysis feasible while preserving the essence of the problem:

- i) the geometric parameters of elements (such as edge lengths and minimum singular values—see below) within one layer Ω_i differ no more than by a fixed constant factor;
- ii) numerical constants independent of the essential parameters of the problem are not examined;
- iii) the asymptotic expansion of the potential at infinity starts with the monopole term, $u = O(1/r)$.

Assumption iii) will later be dropped (Section IV-D). Assumptions i), ii) could be relaxed somewhat, but at a considerable expense of simplicity and clarity.

For problem (2) it is natural to measure the error in the energy seminorm:

$$|u|_E \equiv \left(\int_{\Omega} \sigma |\nabla u|^2 d\Omega \right)^{1/2}$$

The numerical error has two components: the first one is due to the truncation of the domain at r_m , the second one is due

¹It is only under this assumption that the infinite series in [7] converge to the actual values of the potential.

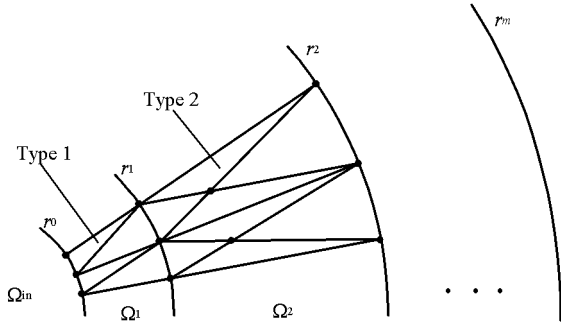


Fig. 2. Ballooning.

to the FE approximation of the exact solution in the truncated region:

$$|u_\infty - u_h|_E \leq |u_\infty - u_{\text{trunc}}|_E + |u_{\text{trunc}} - u_h|_E \quad (5)$$

where u_∞ and u_{trunc} are the exact solutions in the unbounded and truncated domains, respectively; u_h is the FE solution in the truncated region.

The FE solution error in the i th element layer $r_{i-1} \leq r \leq r_i$ can be estimated as

$$|u_{\text{trunc}} - u_h|_{E,i} \propto \sigma_{\min}^{-1} h_i \|u_{\text{trunc}}\|_{H^2,i} \quad (6)$$

where h_i is the element diameter in the i th layer, and σ_{\min} is the minimum singular value of the element edge shape matrix [11] [due to assumption i), it does not matter which element within the layer is taken]. The use of the minimum singular value estimate, as opposed to, say, the inscribed sphere criterion [12], is essential. For a ‘‘wedge-like’’ element, like Type 1 in Fig. 2, the minimum singular value estimate is much more precise than the inscribed sphere estimate (see [13] for details). At the same time, any error estimate would indicate poor approximation accuracy for a ‘‘flat’’ element, like Type 2 in Fig. 2.

The H^2 -norm of the exact solution in the right hand side of (6) is evaluated under assumptions i–iii):

$$\begin{aligned} \|u_{\text{trunc}}\|_{H^2,i}^2 &\propto \|1/r\|_{H^2,i}^2 \propto \|1/r^3\|_{L^2,i}^2 \propto \int_{\Omega_i} (r^{-3})^2 d\Omega \\ &\propto \int_{r_{i-1}}^{r_i} r^{-4} dr \propto r_{i-1}^{-3} - r_i^{-3} \end{aligned}$$

Substituting into (6), we obtain

$$|u_{\text{trunc}} - u_h|_{E,i}^2 \propto \sigma_{\min}^{-2} h_i^2 (r_{i-1}^{-3} - r_i^{-3})$$

The global error in the exterior region is thus found from

$$\begin{aligned} |u_{\text{trunc}} - u_h|_E^2 &= \sum_{i=1}^m |u_{\text{trunc}} - u_h|_{E,i}^2 \\ &\propto \sum_{i=1}^m \sigma_{\min}^{-2} h_i^2 (r_{i-1}^{-3} - r_i^{-3}) \end{aligned}$$

As an illustration, assume a practical scenario that the radii r_i increase in a geometric progression, i.e. $r_i = r_0 q^i$ for some $q > 1$, and each ‘‘ballooning’’ layer is evenly subdivided into k_i sublayers of elements (sublayers not shown in Fig. 2 for simplicity). Then $h_i = (r_i - r_{i-1})/k_i$, and therefore

$$|u_{\text{trunc}} - u_h|_E^2 \propto \sigma_{\min}^{-2} r_0^{-1} q(q-1)^2 (1-q^{-3}) \sum_{i=1}^m q^{-i}/k_i^2.$$

If in addition $k_i = k = \text{const}$,

$$|u_{\text{trunc}} - u_h|_E^2 \propto \sigma_{\min}^{-2} r_0^{-1} q(q-1)(1-q^{-3})(1-q^{-m})/k^2 \quad (7)$$

We can now turn to the truncation error $|u_\infty - u_{\text{trunc}}|_E$ in (5). If the ‘‘ballooning’’ boundary Γ_m is spherical, for the monopole term the truncation error $|u_\infty - u_{\text{trunc}}|_E$ is zero because $u_\infty - u_{\text{trunc}} \propto 1/r_m$ and therefore $\nabla u_\infty - \nabla u_{\text{trunc}} = 0 + \dots$. The truncation error is then due to the leading multipole term $p(p \geq 2)$ and its order of magnitude can be shown to be

$$|u_\infty - u_{\text{trunc}}|_E^2 \propto r_m^{-(2p-1)} = r_0^{-2p+1} q^{(-2p+1)m} \quad (8)$$

The asymptotics of the total error (5) is thus

$$\begin{aligned} |u_\infty - u_h|_E &\propto \frac{\sigma_{\min}^{-1}}{k} (r_0^{-1} q(q-1)(1-q^{-3})(1-q^{-m}))^{1/2} \\ &\quad + (r_0^{-2p+1} q^{(-2p+1)m})^{1/2} \end{aligned} \quad (9)$$

The approximation error is a monotonically increasing function of q , while the truncation error is a decreasing function of q . Thus an optimal value of q exists that minimizes the error (9).

C. An a priori Accuracy Estimate for Spatial Mappings

With the coordinate transformation given by (1) and with the assumed asymptotic behavior of the potential $u \propto 1/r$, one observes that the potential is (approximately) a linear function of the new variable \tilde{r} :

$$u \propto \frac{R_\infty(\theta, \varphi) - \tilde{r}(\theta, \varphi)}{R_0(\theta, \varphi)(R_\infty(\theta, \varphi) - R_0(\theta, \varphi))} \quad (10)$$

According to (6), the energy norm of the FE solution error depends on the H^2 -norm of u , that is, primarily on the magnitude of the second derivatives of u . From (10), one notes that $\partial^2 u / \partial \tilde{r}^2 = 0$. Expressions for the angular derivatives are quite cumbersome, but qualitatively

$$\frac{\partial^2 u}{\partial \alpha^2} \propto \frac{\partial^2 R_\infty}{\partial \alpha^2} + \frac{\partial R_\infty}{\partial \alpha} \frac{\partial R_0}{\partial \alpha} + \frac{\partial^2 R_0}{\partial \alpha^2}, \quad (\alpha = \theta, \varphi)$$

(and a similar relationship for $\partial^2 u / \partial \theta \partial \varphi$).

It is then clear that the best approximation will generally be achieved for spherical artificial boundaries, when R_0 and R_∞ are independent of the angles. This result is corroborated by the numerical experiments of Section VI.

D. Higher Multipole Moments

We briefly consider the case (typical for magnetostatic problems) when the monopole term is absent and the expansion of the solution starts with a higher moment: $u \propto f(\theta, \varphi)/r^p$ ($p \geq 2$).

a) Ballooning. Repeating the previous analysis, one obtains, in lieu of (9):

$$\begin{aligned} |u_\infty - u_h|_E &\propto \frac{\sigma_{\min}^{-1} (q-1)}{k} \\ &\quad \cdot \left(r_0^{-2p+1} (1-q^{-2p+1}) \frac{1-q^{(-2p+1)(m-1)}}{1-q^{-2p+1}} \right)^{1/2} \\ &\quad + (r_0^{-2p+1} q^{(-2p+1)m})^{1/2}. \end{aligned} \quad (11)$$

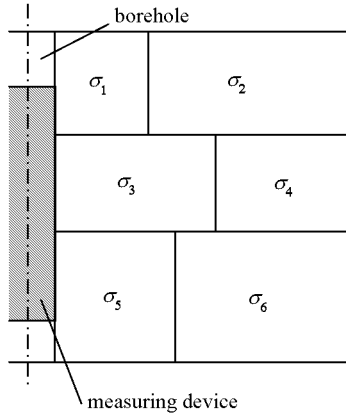


Fig. 3. A schematic representation of the geometric setup.

- b) Spatial mappings. One needs to distinguish between the cases of spherical and nonspherical exterior boundaries Γ_0 , Γ_∞ . If either of these two boundaries is nonspherical, there is no qualitative change in the analysis of Section IV-C: the angular derivatives of R_0 and R_∞ control the H^2 -norm of the solution. However, if both Γ_0 , Γ_∞ are spherical, the accuracy deteriorates compared to the monopole case. The main reason for this deterioration is not that $\partial^2 u / \partial \tilde{r}^2$ is no longer close to zero (that could be rectified by redefining the spatial mapping $r \rightarrow \tilde{r}$) but that the angular derivatives of the solution are necessarily nonzero.²

V. GEOPHYSICAL APPLICATIONS

In oil exploration, a measuring device is moved in the borehole to test the characteristics of underground formations (Fig. 3). We shall consider here galvanic tools measuring dc currents in the ground. Such tools bear several electrodes, some of which have fixed potentials and act as sources, while others have floating (unknown) potentials. The conductivity of the ground formations may be inferred from electrode voltages and currents. The axial length of the tool is usually 10–20 feet, the diameter is 2–8 inches, while the electrode sizes can be less than an inch. The difference in the characteristic sizes leads to an extremely large number of finite elements.

Moreover, the domain is unbounded. Integral equations are not well suited for the multilayered media, the complex tool geometry and deviated (nonvertical) boreholes. The nonuniformity of the outer region (due to the presence of ground layers) presents a serious problem for hybrid FEM-BEM methods as well. This is why the FE method with spatial mappings of unbounded domains and with fast solvers appears promising. The method can also be extended to induction logging (eddy currents in the ground), but this is beyond the scope of the paper.

VI. NUMERICAL EXPERIMENTS

A. General Setup

The numerical tests below illustrate the advantages and the disadvantages of spatial transforms. Two different cases were considered (Fig. 4):

²The equivalence sign $X \propto Y$ implies that the ratio X/Y is bounded, with the bounds independent of any parameters of interest.

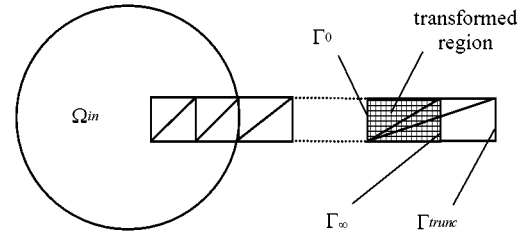


Fig. 4. Test meshes for the problem with open boundaries.

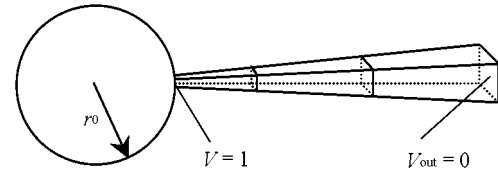


Fig. 5. A spherical sector.

TABLE I
A UNIFORMLY CHARGED SPHERE IN AIR

Test case	Number of unknowns ³	Number of iterations	Time, s	Error, %
Truncation $R_{trunc} = 12\text{m}$	74,273	18	69	8.3
Truncation $R_{trunc} = 50\text{m}$	74,273	142	204	2.7
Spatial mapping $R_0 = 10\text{m}$, $R_\infty = 12\text{m}$	74,273	102	156	1.6

- a) The domain is truncated at an artificial exterior boundary Γ_{trunc} where the homogeneous Dirichlet condition is imposed. The distance to the truncation boundary in the experiments may vary.
- b) The spatial mapping of [6] described in Section III-A is considered. For simplicity we take $R_\infty = cR_0$, $c = \text{const}$. The homogeneous Dirichlet condition is imposed on Γ_∞ .

B. A Uniformly Charged Sphere in Air

This problem has a very simple analytical solution $V = (4\pi r_0^2 \nu / 4\pi \epsilon_0 r) = (r_0^2 \nu / \epsilon_0 r)$, or $V = 1/r$, if we assume $r_0 = 1$ and $\nu / \epsilon_0 = 1$, where r_0 is the radius of the sphere and ν is the surface charge density. Since the potential is exactly $1/r$ and doesn't depend on the angles this case is ideal for the spatial transform. Due to symmetry, only one spherical sector of 10 degrees is modeled (Fig. 5).

The relative error ϵ is evaluated in the energy seminorm:

$$\epsilon = |u_h - u_\infty|_E / |u_\infty|_E.$$

Table I summarizes the results for tests a) and b).³

The spatial transform appreciably improves the accuracy—the effect that cannot be achieved by simply extending

³In Tables I–III the numbers of unknowns and iterations refer to the last level of mesh refinement (finest mesh). The time is the total time of the multilevel solution including mesh refinement and matrix assembly.

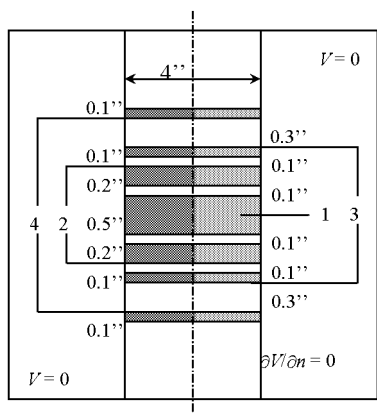


Fig. 6. The model problem.

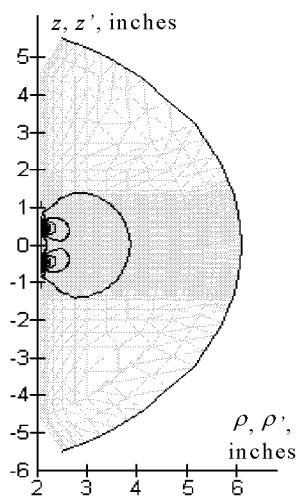


Fig. 7. Equipotential lines and mesh for the model problem (2-D view).

the outer boundary while keeping the number of degrees of freedom the same.

Unfortunately, there is a trade-off for the higher accuracy. The method with the transform converges more slowly due to “bad” element shapes. Indeed, the elements in the transformed region are the mappings of fictitious quite narrow and long elements—obviously, not the best choice for a FE mesh.

C. A Sample Geophysical Problem

The test problem resembles the actual geophysical configuration, with the measuring tool shrunk along the vertical axis. Several insulated conducting rings on a dielectric cylinder serve as electrodes (Fig. 6). Two electrodes labeled with the same number are electrically connected and have the same potential. The medium is uniform with the conductivity $\sigma = 1 S/m$. The problem is axisymmetric, so the modeling was done in the cylindrical sector (1/126th part of the full circle).

Fig. 7 shows a 2-D cross-section of the equipotential lines with electrode #2 having potential $V = 1$ and all other electrodes grounded.

The quasi-analytical matrix R of resistances between electrodes is available for this problem and is used to evaluate the accuracy of FE simulations. The error is computed as the ratio

TABLE II
LOCAL AND GLOBAL MESH REFINEMENT FOR DOMAIN TRUNCATION

R_{trunc} , inches	Global refinement		Local adaptive refinement	
	Unknowns	Error, %	Unknowns	Error, %
6	120,321	19.5	51,323	20
12	128,529	7.53	57,632	8.03
24	130,329	3.24	54,313	3.79
48	130,329	1.93	59,130	2
96	130,329	1.9	45,761	1.31
200	130,329	2.09	49,498	1.29

TABLE III
SPATIAL MAPPING VERSUS TRUNCATION

Description of the test	Unknowns	Time, s ⁴	Error, %
Truncation, $R_{trunc} = 96''$ global refinement	130,329	772	1.9
Truncation, $R_{trunc} = 96''$ local refinement	45,761	561	1.31
Spatial mapping, $R_0 = 5''$, $R_\infty = 6''$, global refinement	122,625	331	1.64
Spatial mapping, $R_0 = 5''$, $R_\infty = 6''$ local refinement	44,908	113	0.88

of matrix norms $\varepsilon = \|R_h - R\|/\|R\|$, where R_h is the matrix of resistances computed by finite element modeling.

The effects of domain truncation and the spatial mapping were tested. Results for the truncation are shown in Table II. Global and local adaptive mesh refinements are compared. The total error comprises the domain truncation error and the FE discretization error. For small R_{trunc} , when the error is primarily due to the truncation of the domain, both refinement techniques are equivalent. For larger distances the discretization error of the global refinement would tend to increase due to the increased element size. But adaptive refinement automatically adjusts the mesh density thus keeping the discretization error small.

However, even though the error can be reduced substantially by increasing the truncation distance, badly shaped long and thin elements cause a substantial increase in the computational time. Changing R_{trunc} from 6 to 200 inches requires about 15 times longer simulations. Further extension of the outer boundary makes the computation impractical.

Table III⁴ compares the spatial mapping with truncation. The advantage of the mapping coupled with local refinement is evident.

In a typical simulation with the spatial transform the solution time is approximately proportional to the number of unknowns.

Fig. 8 shows convergence results for the sample geophysical problem of Fig. 6, with three different electrodes “active” (i.e., having a unit potential, with all other electrodes grounded).

However, there is a trade-off between the solution accuracy and the convergence rate of the multigrid solver. When traditional adaptivity procedures (see [5]) are applied in the transformed region, the effective mesh quality tends to deteriorate, impeding multigrid convergence. Investigation of

⁴For a 400 MHz Pentium II

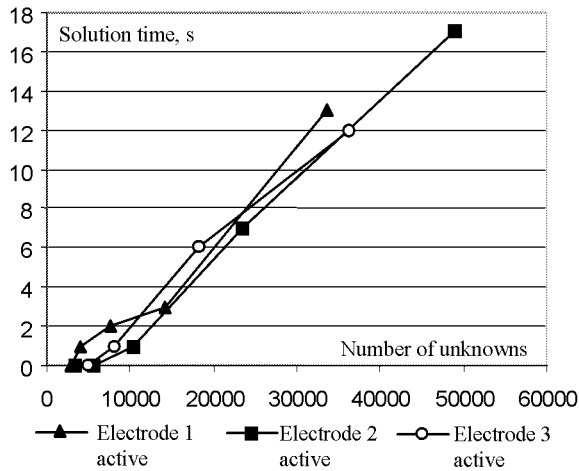


Fig. 8. Convergence results for the spatial transform.

alternative adaption techniques and local error estimators for the transformed region is worthwhile and is planned for future research.

VII. CONCLUSIONS

- 1) The proposed combination of adaptive multigrid algorithms with spatial transforms is a viable method for solving static open boundary problems.
- 2) The method is especially effective when the artificial boundaries of the transformed region can be chosen to be spherical and when the expansion of the potential at infinity starts with the monopole term. More research is needed to improve the convergence rate of the multigrid solver in other cases.

- 3) The following methodological principle should be emphasized: the approximation accuracy is a key factor in the comparison of different finite element techniques for open boundary problems.

REFERENCES

- [1] Q. Chen and A. Konrad, "A review of finite element open boundary techniques for static and quasistatic electromagnetic field problems," *IEEE Trans. Magn.*, vol. 33, no. 1, pp. 663–676, 1997.
- [2] S. Gratkowski, "Infinite elements for axisymmetric electrical field problems with open boundaries," *COMPEL*, vol. 17, no. 5–6, p. 781, 1998.
- [3] J. Xu, "Iterative methods by space decomposition and subspace correction," *SIAM Review*, vol. 34, no. 4, pp. 581–613, 1992.
- [4] J. H. Bramble, J. E. Pasciak, and J. Xu, "Parallel multilevel preconditioners," *Math. Comp.*, vol. 55, no. 191, pp. 1–22, 1990.
- [5] I. Tsukerman and A. Plaks, "Hierarchical basis multilevel preconditioners for 3D magnetostatic problems," *IEEE Trans. Magn.*, vol. 35, no. 3, pp. 1143–1146, 1999.
- [6] A. Stochniol, "A general transformation for open boundary finite element method for electromagnetic problems," *IEEE Trans. Magn.*, vol. 28, no. 2, pp. 1679–1681, 1992.
- [7] J.-P. Berenger, "A perfectly matched layer for the absorption of electromagnetic waves," *J. Comput. Phys.*, vol. 114, pp. 185–200, 1994.
- [8] S. Abarbanel and D. Gottlieb, "A mathematical analysis of the PML method," *J. Comput. Phys.*, vol. 134, pp. 357–363, 1997.
- [9] Z. S. Sacks, D. M. Kingsland, R. Lee, and J. F. Lee, "A perfectly matched anisotropic absorber for use as an absorbing boundary condition," *IEEE Trans. on Ant. Prop.*, vol. 43, no. 12, pp. 1460–1463, 1995.
- [10] I. Titar, O. Biro, and K. Preis, "A proof of the perfect matching property of PML's in static fields," *IEEE Trans. Magn.*, vol. 35, no. 3, pp. 1139–1142, 1999.
- [11] I. A. Tsukerman, "Approximation of conservative fields and the element 'edge shape matrix'," *IEEE Trans. Magn.*, vol. 34, pp. 3248–3251, 1998.
- [12] V. N. Parthasarathy, C. M. Graichen, and A. F. Hathaway, "A comparison of tetrahedron quality measures," *Finite Elements in Analysis and Design*, vol. 15, pp. 255–261, 1993.
- [13] I. A. Tsukerman and A. Plaks, "Comparison of accuracy criteria for approximation of conservative fields on tetrahedra," *IEEE Trans. Magn.*, vol. 34, pp. 3252–3255, 1998.